Coincidence-conditioned Compton-modulation recovery from annihilation Bell pairs

Peter Caradonna [1,*] Kenji Shimazoe [1,2,†] and Takeshi Sato [1,3,4,‡]

[1]*Department of Nuclear Engineering and Management, The University of Tokyo, Bunkyo-ku, Tokyo, Japan*
[2]*Department of Bioengineering, The University of Tokyo, Bunkyo-ku, Tokyo, Japan*
[3]*Photon Science Center, Graduate School of Engineering, The University of Tokyo, Bunkyo-ku, Tokyo, Japan*
[4]*Research Institute for Photon Science and Laser Technology, The University of Tokyo, Bunkyo-ku, Tokyo, Japan*

(Received 27 May 2026; accepted 28 October 2026; published 16 November 2026)

We develop an idealized framework for recovering coincidence-conditioned Compton-modulation levels from 511 keV photon pairs produced in electron-positron annihilation and described by a Bell state. Compton scattering followed by angular postselection in the signal arm defines a coincidence-conditioned idler ensemble whose degree of polarization is determined by the selected signal-arm scattering angle. The ensemble is analyzed through the azimuthal modulation of the idler Compton-scattering distribution. Two prescribed signal-arm angles, $\alpha_1 = 45^\circ$ and $\alpha_2 = 81.7^\circ$, give ideal narrow-signal-channel, full-polar-angle relative modulation depths of approximately 0.109 62 and 0.237 58, respectively, and thereby define a binary discrimination task. Time-tagged coincidence data are partitioned into successive acquisition intervals, and each interval is classified using an unbiased estimator of its idler modulation depth. For the prescribed pair $\alpha_1 = 45^\circ$ and $\alpha_2 = 81.7^\circ$, a finite-statistics analysis gives a conservative event requirement of approximately 2×10^3 retained coincidences per interval for the two-sided 95% separation criterion used here. More generally, the required count increases rapidly as the two modulation levels approach one another. Finite angular acceptance, reconstruction resolution, and azimuthally uniform uncorrelated background are incorporated through a reconstructed modulation depth, while the corresponding acquisition timescale depends additionally on the retained coincidence rate. The resulting framework provides an operational Bell-state baseline for coincidence-conditioned Compton-modulation recovery and for assessing detector-dependent departures from the ideal response.

DOI: 10.1103/2183-1hsp

I. INTRODUCTION

In optical quantum-information experiments, polarization correlations can be analyzed using nearly projective measurements and reconstructed by quantum-state tomography. Controlled coupling of polarization to unresolved temporal or path degrees of freedom has demonstrated entanglement sudden death, the separation between the loss of Bell nonlocality and entanglement, and the redistribution of entanglement between photons and their effective environments [1,2]. A closer operational analog is optical remote-state preparation, in which a local measurement on one photon of a parametric-down-conversion pair identifies a coincidence-conditioned polarization ensemble for its partner through a classical measurement record [3,4]. Such protocols conditionally select a remote subensemble without changing the unconditional remote state. Their implementation, however, relies on nearly projective polarization measurements that are unavailable for high-energy photons.

For the two-photon annihilation channel of an electron-positron spin-singlet state at rest, the emitted photons each have an energy of 511 keV. At this energy, Compton scattering replaces conventional polarization projectors and constitutes a nonprojective generalized measurement. The predicted Bell-state polarization correlations are identified indirectly as a modulation of the joint Compton-scattering rate with the relative azimuthal angle between the two scattering planes [5–10]. Polarization information is therefore inferred statistically from an ensemble of scattering directions through the Klein-Nishina azimuthal response [11]. The recovered modulation depends on both the incident two-photon state and the complete polarimeter response, including the kinematic analyzing power, detector acceptance, angular and energy resolution, event reconstruction, and coincidence selection [10,12].

Modern segmented detectors have established that these correlations can be resolved experimentally, while also exposing the efficiency and statistical limitations of Compton polarimetry at 511 keV. Makek *et al.* demonstrated the dependence of the measured modulation on the accepted polar-angle range and azimuthal resolution [9]. Related developments have investigated annihilation-photon correlations in dedicated polarimeters and positron-emission tomography (PET) [10,12,13]. Kim *et al.* incorporated detector segmentation, energy resolution, angular uncertainty, and backgrounds into a coincidence-reconstruction framework, although the retained double-Compton rate was only a small fraction

*Contact author: petercaradonna65@gmail.com
†Contact author: shimazoe@g.ecc.u-tokyo.ac.jp
‡Contact author: sato@atto.t.u-tokyo.ac.jp

Published by the American Physical Society under the terms of the Creative Commons Attribution 4.0 International license. Further distribution of this work must maintain attribution to the author(s) and the published article's title, journal citation, and DOI.

of the corresponding conventional PET rate [13]. Bordes *et al.* subsequently resolved modulation changes following an intermediate Compton interaction while treating detector acceptance and multiple-scattering backgrounds [14]. These studies demonstrate that the measured modulation is a convolution of the underlying polarization correlations with the detector response and, importantly for the present work, that distinct modulation levels can nevertheless be resolved experimentally when detector effects and counting statistics are adequately controlled.

The interpretation of the measured modulation nevertheless requires care. Tkachev *et al.* corrected the azimuthal visibility by the product of the two single-scatter analyzing powers and denoted the resulting quantity by C_{vis}. Using an approximate pure-state construction, they argued that this quantity tracks the concurrence of the postscattering polarization state [15]. Applied to the randomized perpendicular-polarization mixture considered by Bohm and Aharonov, however, the same prescription gives $C_{\mathrm{vis}} = 1/2$, although the state is separable and its concurrence is zero [15,16]. Thus, C_{vis} measures normalized azimuthal-correlation strength and cannot generally be identified with concurrence. An explicitly reconstructed, angle-conditioned two-photon polarization density matrix instead predicts a finite near-right-angle interval of zero concurrence [17], while a successive-scattering extension finds, for the geometries considered, broader zero-concurrence regions even though the ℓ_1 norm of coherence in the chosen polarization basis can remain finite [18].

These conclusions follow from different state constructions and inference procedures. More generally, neither a $\cos(2\phi)$ correlation nor a Bohm-Aharonov enhancement ratio constitutes, without additional state assumptions, an entanglement witness over the full set of separable states. Related separable-state ambiguities and their dependence on the measurement configuration had been identified previously [19,20]. A recent positive-operator-valued-measure analysis exhibited general separable states reproducing commonly used Compton-correlation signatures and distinguished such model-dependent discriminators from entanglement witnesses and Bell tests [21]. The authors clarified, however, that these counterexamples are not symmetry-respecting annihilation-photon alternatives and that the Bohm-Aharonov criterion remains meaningful within the physically constrained class for which it was formulated [22]. Accordingly, the modulation levels considered here are interpreted only within an explicitly specified Bell-state and Compton-response model.

Within this model-specific setting, Ref. [23] compared the coincidence-conditioned polarization response of a Bell state with that of a separable Bohm-Aharonov mixture constructed to reproduce the same average spin-angular-momentum conservation. The equality between the degrees of polarization of the scattered signal ensemble and its coincidence-conditioned idler ensemble was subsequently shown to hold if and only if the initial state is Bell equivalent within the class considered in Ref. [24]. This result supplies a model-specific Bell-state baseline but does not specify how its predicted modulation can be recovered from finite time-tagged Compton data. Existing studies have addressed angular correlations, detector response, or polarization-state evolution, but not the restricted operational task considered here, which is to discriminate two prescribed coincidence-conditioned modulation levels generated by two signal-arm scattering settings.

We develop an idealized operational framework for this task. A signal control station selects between the prescribed settings $\alpha_1 = 45^\circ$ and $\alpha_2 = 81.7^\circ$, where the latter corresponds, to the quoted angular precision, to the maximum Compton analyzing power at 511 keV [25]. An idler analysis station independently records the arrival times and Compton-scattering directions of the partner photons. Once the signal-side time tags are available, the idler event stream is partitioned into acquisition intervals and coincidence selection retains the idler events associated with accepted signal detections. The azimuthal distribution in each interval is then analyzed to estimate its modulation depth and classify it relative to the two predicted modulation levels. Because the unconditional idler ensemble remains unpolarized, the idler record alone contains no modulation signature of the prescribed sequence. Recovery of that sequence from the idler data requires the classical signal record and coincidence postselection. We derive the relevant angular distributions, examine the information lost through marginalization over the idler polar angle, quantify the event statistics required for classification as a function of the separation between the prescribed modulation levels, assess the effects of finite acceptance, angular resolution, accidental coincidences, and azimuthally uniform detector backgrounds, and identify the need for forward detector simulation to treat structured backgrounds and multiple scattering. The framework is therefore an operational study of Bell-state-conditioned Compton-modulation recovery, not a practical communication system, Bell-inequality test, or standalone entanglement-verification protocol.

Beyond this specific task, the framework may provide an operational foundation for future tests of the Bell-orbit polarization symmetry identified in Ref. [24] for high-energy photon pairs lacking conventional projective polarization measurements.

II. GEOMETRY AND THEORY

This section proceeds in three stages. First, we establish the Bell-state geometry and signal-side selection, then derive the angular response of the corresponding coincidence-conditioned idler ensemble. Second, we reduce the full angular response to a finite-acceptance azimuthal profile and identify the modulation depth that distinguishes the two prescribed signal settings. Third, we incorporate finite detector acceptance, angular reconstruction, and background effects to connect the ideal modulation to its reconstructed counterpart.

A. Conditional geometry and angular response

We consider an electron-positron annihilation source that emits back-to-back pairs of 511 keV photons in the Bell state $|\Psi^-\rangle$, written in the circular-polarization basis as [20]

$$|\Psi^-\rangle = \frac{1}{\sqrt{2}}\,|R_i\rangle \otimes |R_s\rangle - \frac{1}{\sqrt{2}}\,|L_i\rangle \otimes |L_s\rangle\,.$$

Here, $|R\rangle$ and $|L\rangle$ denote right- and left-circular polarization states, and the subscripts i and s label the idler and signal photons, respectively. As illustrated in Fig. 1, the collimator

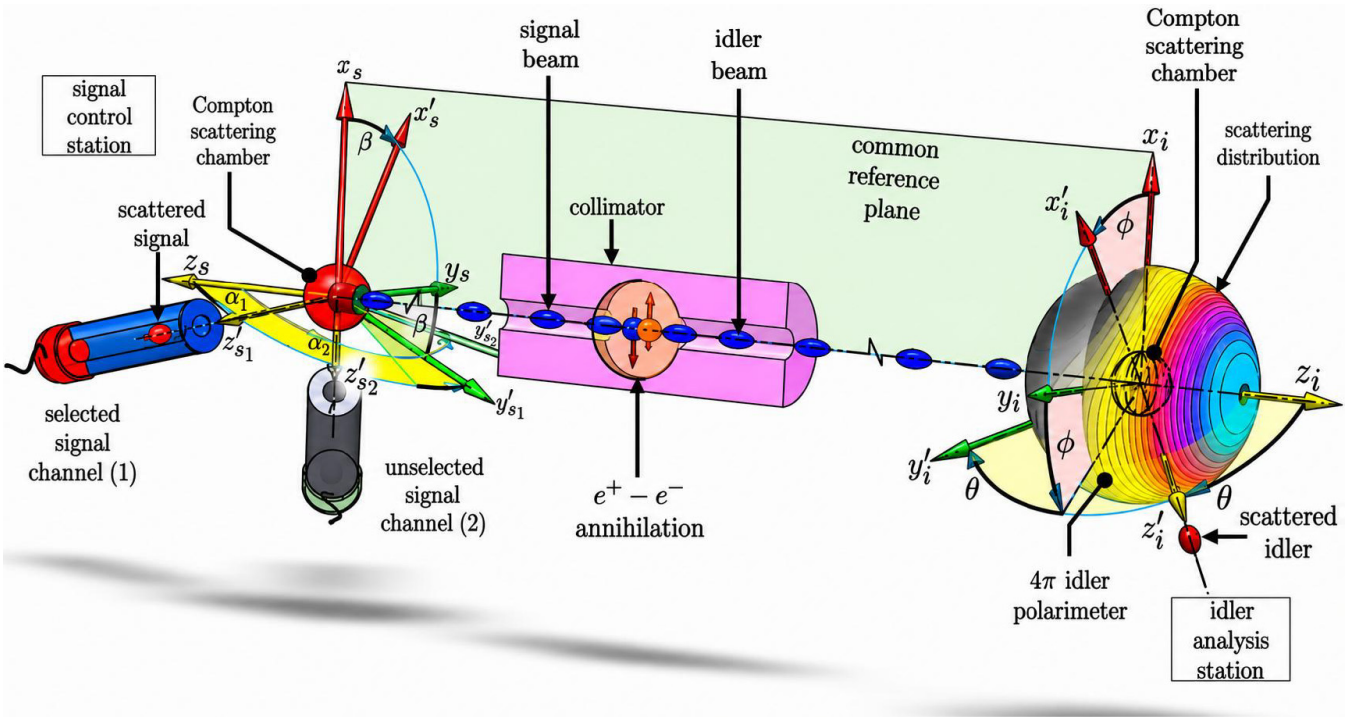


FIG. 1. Idealized coincidence-measurement geometry for Compton-scattered annihilation photons. A back-to-back pair of 511 keV photons is collimated into signal and idler arms defined relative to a common reference plane containing the x_s and x_i axes. At the signal control station, the scattered signal photon is accepted into one of two fixed channels at polar angles α_1 or α_2. The angle β specifies the azimuthal orientation of the selected signal scattering plane relative to the common reference plane. Coincidence selection using detections in the selected signal channel defines the corresponding idler ensemble. At the idler analysis station, an idealized 4π Compton polarimeter records the idler scattering direction parametrized by (θ, ϕ). The colored surface visualizes the idler angular scattering density derived below, which is normalized over the full solid angle. Primed axes denote the corresponding local scattering frames, with each z' axis aligned with the associated scattered-photon direction.

defines the signal and idler propagation arms relative to a common reference plane containing the x_s and x_i axes. The two photons then propagate to the signal control and idler analysis stations, respectively. Primed axes denote the corresponding local scattering frames, with each z' axis aligned with the associated scattered-photon direction.

Let $\rho = |\Psi^-\rangle\langle\Psi^-|$. Following Ref. [23], the corresponding 4×4 Stokes matrix is

$$S(\rho) = \begin{pmatrix} 1 & 0 & 0 & 0 \\ 0 & -1 & 0 & 0 \\ 0 & 0 & 1 & 0 \\ 0 & 0 & 0 & 1 \end{pmatrix}.$$

In the geometry shown in Fig. 1, the signal photon undergoes Compton scattering at the signal control station and is then accepted into one of two fixed channels labeled by (α_j, β), with $j = 1, 2$. The angle α_j defines the polar scattering angle of the selected channel, while β defines the azimuthal orientation of its scattering plane relative to the common reference plane. For $\beta = 0$, the primed signal axis x_s' is aligned with the unprimed idler axis x_i. Coincidence selection using detections in the selected signal channel defines the partner idler ensemble associated with that setting. More generally, the two channels could have different azimuthal orientations, in which case separate angles β_j would be required. Here, a common azimuthal orientation is assumed, so that $\beta_1 = \beta_2 = \beta$. The Stokes matrix after signal-arm scattering through (α_j, β) is [23]

$$S'(\rho) = S(\rho)M(-\beta)T_{\rm un}(\alpha_j), \tag{1}$$

where

$$M(-\beta) = \begin{pmatrix} 1 & 0 & 0 & 0 \\ 0 & \cos 2\beta & -\sin 2\beta & 0 \\ 0 & \sin 2\beta & \cos 2\beta & 0 \\ 0 & 0 & 0 & 1 \end{pmatrix} \tag{2}$$

relates the Stokes parameters in the two coordinate systems.

We express photon energies in units of the electron rest energy, so that $E_{0s} = E_{0i} = 1$ for the 511 keV annihilation photons considered here. With the incident signal-photon energy therefore fixed at $E_{0s} = 1$, the Mueller matrix for Compton scattering by unpolarized electrons takes the form

$$T_{\rm un}(\alpha_j) = \frac{r_0^2}{2}E^2(\alpha_j) \times \begin{pmatrix} t_{11}(\alpha_j) & t_{12}(\alpha_j) & 0 & 0 \\ t_{12}(\alpha_j) & 2 - t_{12}(\alpha_j) & 0 & 0 \\ 0 & 0 & t_{33}(\alpha_j) & 0 \\ 0 & 0 & 0 & t_{44}(\alpha_j) \end{pmatrix}. \tag{3}$$

Here, $r_0 = 2.82 \times 10^{-15}$ m is the classical electron radius. The standard Compton kinematic prefactor $[E(\alpha_j)/E_{0s}]^2$ has reduced to $E^2(\alpha_j)$ because $E_{0s} = 1$. For a photon of unit

incident energy Compton scattered through a generic polar angle χ,

$$E(\chi) = \frac{1}{2 - \cos\chi},$$

and the matrix elements required explicitly in the subsequent analysis are

$$t_{11}(\chi) = 1 + \cos^2\chi + (1 - E(\chi))(1 - \cos\chi),$$
$$t_{12}(\chi) = \sin^2\chi.$$

The remaining Mueller-matrix elements $t_{33}(\chi)$ and $t_{44}(\chi)$ are retained here for completeness, but their explicit functional forms do not enter the quantities evaluated below and are given in Ref. [26].

Within the two-photon Stokes-matrix convention of Ref. [23], the first column and first row of $S'(\rho)$ in Eq. (1) give the conditional local Stokes vectors in the signal ($|S'_s(\alpha_j)\rangle$) and idler ($|S'_i(\alpha_j, \beta)\rangle$) arms, respectively. One obtains

$$|S'_s(\alpha_j)\rangle = \frac{r_0^2}{2} E^2(\alpha_j) t_{11}(\alpha_j) \begin{pmatrix} 1 \\ p(\alpha_j) \\ 0 \\ 0 \end{pmatrix} \tag{4a}$$

and

$$|S'_i(\alpha_j, \beta)\rangle = \frac{r_0^2}{2} E^2(\alpha_j) t_{11}(\alpha_j) \begin{pmatrix} 1 \\ -p(\alpha_j)\cos(2\beta) \\ p(\alpha_j)\sin(2\beta) \\ 0 \end{pmatrix}. \tag{4b}$$

Here, for a generic Compton polar scattering angle χ, we define

$$p(\chi) = \frac{t_{12}(\chi)}{t_{11}(\chi)} = \frac{(2 - \cos\chi)\sin^2\chi}{3 - \cos\chi(3 - 3\cos\chi + \cos^2\chi)}. \tag{5}$$

In the Stokes-vector convention used in Ref. [23], the degree of polarization is the magnitude of the polarization Stokes vector normalized by its intensity component. For the Bell-state photons considered here, the Stokes vectors in Eqs. (4a) and (4b) both give $\sqrt{S_1^2 + S_2^2 + S_3^2}/S_0 = p(\alpha_j)$ [23,24]. Thus, for each fixed α_j, $p(\alpha_j)$ is the degree of polarization of both the scattered signal ensemble and the coincidence-conditioned idler ensemble. The same ratio $t_{12}(\chi)/t_{11}(\chi)$ is also the single-scatter Compton analyzing power for the response used here.

The coincidence-conditioned idler Stokes vector $|S'_i(\alpha_j, \beta)\rangle$ is realized operationally through the timing and postselection procedure described later in Secs. III and IV.

For 511 keV photons, the analyzing power $p(\chi)$ in Eq. (5) increases over $0 \leqslant \chi \lesssim 81.66^\circ$, reaches its maximum $p_{\max} \simeq 0.6918$ at $\chi \simeq 81.66^\circ$, as obtained from $dp(\chi)/d\chi = 0$, and then decreases slightly to $p(90^\circ) = 2/3$. We therefore choose $\alpha_2 = 81.7^\circ$ as the signal-arm setting corresponding, to the quoted angular precision, to the maximum Compton analyzing power, while $\alpha_1 = 45^\circ$ provides the lower-modulation reference setting used for the baseline two-setting analysis.

The partner idler photons subsequently propagate to the idler analysis station shown on the right of Fig. 1, where they undergo Compton scattering through the polar and azimuthal angles (θ, ϕ). When the recorded idler events are conditioned on coincidences with signal detections in channel j, the corresponding idler ensemble is described by Eq. (4b). The conditional differential cross section for this ensemble is [23]

$$\frac{d\sigma}{d\Omega}(\theta, \phi \mid \alpha_j, \beta) = \langle I | T_{\rm un}(\theta) M(\phi) | S'_i(\alpha_j, \beta)\rangle, \tag{6}$$

where $\langle I| = (1 \quad 0 \quad 0 \quad 0)$ represents a polarization-insensitive photon counter [20]. Here, $M(\phi)$ and $T_{\rm un}(\theta)$ have the same structures as in Eqs. (2) and (3), respectively, but now depend on the idler scattering angles (θ, ϕ).

Substituting Eqs. (2), (3), and (4b) into Eq. (6) gives

$$\frac{d\sigma}{d\Omega}(\theta, \phi \mid \alpha_j, \beta) = B(\alpha_j) E^2(\theta) t_{11}(\theta) \times \left[1 - p(\alpha_j)\frac{t_{12}(\theta)}{t_{11}(\theta)}\cos 2(\phi + \beta)\right], \tag{7}$$

where $p(\alpha_j)$ is the degree of linear polarization of the coincidence-conditioned idler ensemble incident on the analyzer, and where, for compactness, the signal-arm-dependent prefactor is defined as

$$B(\alpha_j) \equiv \frac{r_0^4}{4} E^2(\alpha_j) t_{11}(\alpha_j). \tag{8}$$

The total cross section associated with signal setting α_j is obtained by integrating Eq. (7) over the full solid angle, with $d\Omega = \sin\theta\, d\theta\, d\phi$, $0 \leqslant \theta \leqslant \pi$, and $0 \leqslant \phi \leqslant 2\pi$. This gives

$$\sigma(\alpha_j) = \frac{2\pi}{9} B(\alpha_j)(40 - 27\ln 3). \tag{9}$$

Dividing Eq. (7) by Eq. (9) gives the normalized idler angular scattering density

$$f_\Omega(\theta, \phi \mid \alpha_j, \beta) \equiv \frac{1}{\sigma(\alpha_j)}\frac{d\sigma}{d\Omega}(\theta, \phi \mid \alpha_j, \beta) = \frac{9E^2(\theta) t_{11}(\theta)}{2\pi(40 - 27\ln 3)} \times \left[1 - p(\alpha_j)\frac{t_{12}(\theta)}{t_{11}(\theta)}\cos 2(\phi + \beta)\right]. \tag{10}$$

The density f_Ω is normalized over the full solid angle. The signal-arm prefactor $B(\alpha_j)$ cancels in the normalization, so the dependence on the selected signal setting remains through $p(\alpha_j)$. This density is the quantity visualized by the 4π scattering distribution at the idler analysis station in Fig. 1. Figure 2 shows the forward-hemisphere portion of the same full-sphere normalized density for the two prescribed signal settings at $\beta = 0$.

B. Finite-acceptance azimuthal modulation

For the finite-acceptance construction, it is convenient to retain the differential cross section before normalization. In the present conditional geometry, we construct the

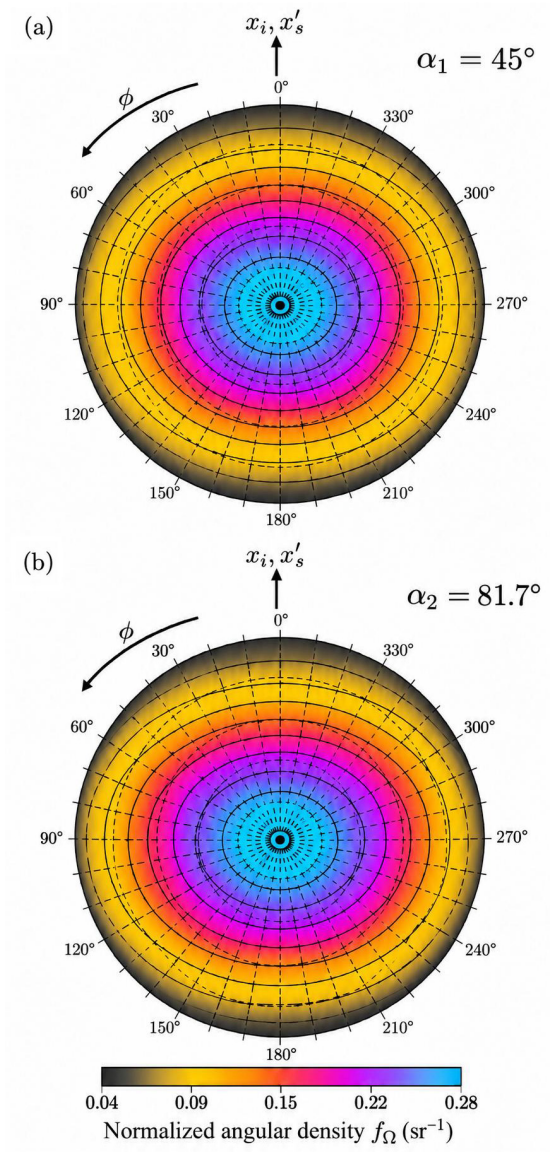


FIG. 2. Forward-hemisphere projections of the normalized coincidence-conditioned idler angular scattering density $f_\Omega(\theta, \phi \mid \alpha_j, \beta)$ evaluated at $\beta = 0$ for (a) $\alpha_1 = 45°$ and (b) $\alpha_2 = 81.7°$. The maps display $0 \leqslant \theta \leqslant \pi/2$ and are projected onto the transverse plane with radial coordinate $\sin\theta$ and azimuthal coordinate ϕ. The color scale gives the value of f_Ω in sr^{-1} at each displayed direction, while the solid black contours denote loci of constant value. For $\beta = 0$, the primed signal axis x_s' is aligned with the unprimed idler axis x_i, which defines the azimuthal reference direction. The density is normalized over the full solid angle even though only the forward hemisphere is displayed. The stronger azimuthal anisotropy for α_2 reflects the larger degree of linear polarization $p(\alpha_2)$ of the coincidence-conditioned idler ensemble.

finite-acceptance azimuthal profile by integrating over the accepted idler polar-angle range $\Delta\theta$.

First, recast Eq. (7) as

$$P(\theta, \phi \mid \alpha_j, \beta) \equiv \frac{d\sigma}{d\Omega}(\theta, \phi \mid \alpha_j, \beta) = P_0\left[1 - \frac{P_2}{P_0}\cos 2(\beta + \phi)\right], \quad (11)$$

where

$$P_0 \equiv P_0(\theta, \alpha_j) = B(\alpha_j)E^2(\theta)t_{11}(\theta),$$
$$P_2 \equiv P_2(\theta, \alpha_j) = B(\alpha_j)E^2(\theta)p(\alpha_j)t_{12}(\theta).$$

For unit incident photon energy, the unpolarized Klein-Nishina differential cross section is

$$\left(\frac{d\sigma}{d\Omega}\right)_{\rm un} = \frac{r_0^2}{2}E^2(\chi)t_{11}(\chi).$$

Since $B(\alpha_j) = (r_0^4/4)E^2(\alpha_j)t_{11}(\alpha_j)$, the coefficient $P_0(\theta, \alpha_j)$ is the product of the corresponding unpolarized differential cross-section factors for the signal and idler scatterings. It therefore represents the azimuthally independent baseline of the coincidence-conditioned profile. The coefficient $P_2(\theta, \alpha_j)$ is the amplitude of the polarization-dependent second-harmonic contribution. Thus, at fixed θ, the fractional modulation is $P_2/P_0 = p(\alpha_j)p(\theta)$. Here, $p(\theta) = t_{12}(\theta)/t_{11}(\theta)$ is the Compton analyzing power of the idler analyzer at polar scattering angle θ.

The 4π idler polarimeter shown in Fig. 1 defines the idealized full-solid-angle reference geometry. A realistic analyzer need not retain the complete polar-angle range. We therefore introduce an accepted idler polar-angle interval before constructing the experimentally relevant azimuthal profile. Let $\Delta\theta = [\theta_-, \theta_+]$ denote the idler polar-angle range accepted by the analyzer. We integrate Eq. (11) over this range.

$$P_{\Delta\theta}(\phi \mid \alpha_j, \beta) \equiv \int_{\theta_-}^{\theta_+} P(\theta, \phi \mid \alpha_j, \beta)\sin\theta\, d\theta = P_{0,\Delta\theta}(\alpha_j) - P_{2,\Delta\theta}(\alpha_j)\cos 2(\beta + \phi), \quad (12)$$

where

$$P_{0,\Delta\theta}(\alpha_j) = B(\alpha_j)\int_{\theta_-}^{\theta_+} E^2(\theta)t_{11}(\theta)\sin\theta\, d\theta,$$
$$P_{2,\Delta\theta}(\alpha_j) = B(\alpha_j)p(\alpha_j)\int_{\theta_-}^{\theta_+} E^2(\theta)t_{12}(\theta)\sin\theta\, d\theta.$$

The quantities $P_{0,\Delta\theta}$ and $P_{2,\Delta\theta}$ are the constant and second-harmonic coefficients of the accepted azimuthal profile.

The integration in Eq. (12) deliberately combines events over the accepted idler polar-angle range. For the normalized angular density in Eq. (10), the azimuthally averaged polar distribution at fixed θ is independent of the selected signal setting α_j and of β, whereas the distinction between the two prescribed settings is carried by the azimuthal modulation. Integrating over $\Delta\theta$ therefore increases the retained coincidence sample relative to a narrow polar-angle selection and improves the raw counting statistics of the azimuthal profile. Whether this reduces the acquisition time required to distinguish the two modulation depths also depends on the corresponding change in the acceptance-weighted modulation separation. The tradeoff is that the θ-dependent analyzing power is replaced by an acceptance-weighted average over $\Delta\theta$, and the event-by-event θ information that could be retained in a full two-dimensional analysis is discarded from the one-dimensional azimuthal marginal.

We define the relative azimuthal profile by

$$R_{\Delta\theta}(\phi \mid \alpha_j, \beta) = \frac{P_{\Delta\theta}(\phi \mid \alpha_j, \beta)}{P_{0,\Delta\theta}(\alpha_j)}.$$

Substituting Eq. (12) then gives

$$R_{\Delta\theta}(\phi \mid \alpha_j, \beta) = 1 - \mu_{\Delta\theta}(\alpha_j)\cos 2(\beta + \phi), \tag{13}$$

where

$$\mu_{\Delta\theta}(\alpha_j) = \frac{P_{2,\Delta\theta}(\alpha_j)}{P_{0,\Delta\theta}(\alpha_j)} = p(\alpha_j)p_{\Delta\theta}. \tag{14}$$

Here,

$$p_{\Delta\theta} = \frac{\int_{\theta_-}^{\theta_+} E^2(\theta)t_{12}(\theta)\sin\theta\, d\theta}{\int_{\theta_-}^{\theta_+} E^2(\theta)t_{11}(\theta)\sin\theta\, d\theta}.$$

Thus, $p_{\Delta\theta}$ is the acceptance-weighted Compton analyzing power of the idler analyzer over $\Delta\theta$.

Equation (13) has the same unit-mean cosine form as the normalized angular-correlation quantity introduced by Kasday *et al.* [7]. In the present conditional construction, however, the finite-acceptance modulation depth $\mu_{\Delta\theta}(\alpha_j) = p(\alpha_j)p_{\Delta\theta}$ follows from the explicit weighted average over the accepted idler polar-angle range. The prefactor $B(\alpha_j)$ cancels from the normalized profile and from the ratio defining $\mu_{\Delta\theta}(\alpha_j)$. Furthermore, since $P_0(\theta, \alpha_j)$ represents the polarization-independent coincidence baseline constructed from the corresponding unpolarized Klein-Nishina differential cross-section factors, $P_{0,\Delta\theta}(\alpha_j)$ is the same baseline after integrating the idler response over the accepted polar-angle range $\Delta\theta$. It is therefore also the azimuthal mean of the accepted profile,

$$\langle P_{\Delta\theta}\rangle_\phi \equiv \frac{1}{2\pi}\int_0^{2\pi} P_{\Delta\theta}(\phi \mid \alpha_j, \beta)\, d\phi = P_{0,\Delta\theta}(\alpha_j).$$

The modulation depth itself therefore does not require knowledge of the total cross section or the absolute source strength.

For the ideal full-polar-angle acceptance $\Delta\theta = [0, \pi]$, Eq. (14) reduces to

$$\mu_{[0,\pi]}(\alpha_j) = \frac{36(\ln 3 - 1)}{40 - 27\ln 3}\, p(\alpha_j).$$

For the two prescribed signal-arm settings,

$$\mu_{[0,\pi]}(45^\circ) \simeq 0.109\,62, \quad \mu_{[0,\pi]}(81.7^\circ) \simeq 0.237\,58.$$

Thus, the corresponding relative modulation depths are approximately 11.0% and 23.8%, with separation

$$\Delta\mu_{[0,\pi]} = \mu_{[0,\pi]}(81.7^\circ) - \mu_{[0,\pi]}(45^\circ) \simeq 0.127\,95.$$

For the prescribed baseline pair $\alpha_1 = 45^\circ$ and $\alpha_2 = 81.7^\circ$, the separation $\Delta\mu_{[0,\pi]}$ provides the ideal reference scale for distinguishing the two signal-arm settings. Figure 3 shows the corresponding full-polar-angle relative azimuthal profiles for the two prescribed signal settings at $\beta = 0$.

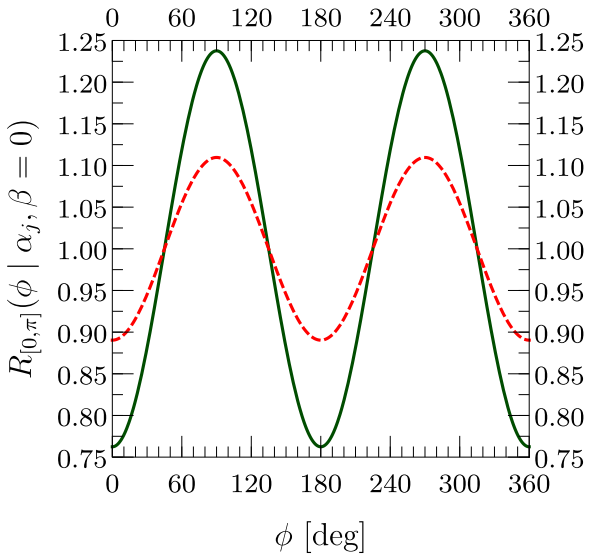


FIG. 3. Full-polar-angle relative azimuthal profiles $R_{[0,\pi]}(\phi \mid \alpha_j, \beta = 0)$ obtained from Eq. (13) for the two prescribed signal settings. The dashed red curve corresponds to $\alpha_1 = 45^\circ$ with $\mu_{[0,\pi]} \simeq 0.109\,62$, and the solid green curve corresponds to $\alpha_2 = 81.7^\circ$ with $\mu_{[0,\pi]} \simeq 0.237\,58$. The figure shows the larger azimuthal modulation produced by the setting corresponding, to the quoted angular precision, to the maximum Compton analyzing power, α_2, while both relative profiles retain unit azimuthal mean.

C. Detector response and reconstructed modulation

The construction through Eq. (13) treats the signal setting α_j as exact and the idler selection as an ideal top-hat interval in the true angle θ. In a physical implementation, finite angular acceptance and finite angular reconstruction resolution are distinct aspects of the detector response, even though both can be influenced by the same detector geometry, segmentation, energy resolution, and event-reconstruction procedure. The finite signal-channel acceptance about α_j and the accepted idler interval $\Delta\theta$ determine which reconstructed events are retained. The reconstruction resolution in α and θ determines how accurately the underlying scattering angles are assigned and therefore governs migration into and out of those accepted angular ranges.

Let $W_j(\alpha)$ be the probability that a signal photon scattered through the true angle α is reconstructed and accepted in channel j, and let $W_{\Delta\theta}(\theta)$ be the probability that an idler photon scattered through the true angle θ is reconstructed inside the selected interval $\Delta\theta$. These response weights incorporate the finite detector dimensions, polar-angle reconstruction kernels, energy-dependent efficiencies, and event-selection cuts. Here, $B(\alpha)$ denotes the signal-arm prefactor defined in Eq. (8) with the discrete setting α_j replaced by the continuous true scattering angle α. For an azimuthally uniform response that factorizes between the two arms, define

$$\overline{p}_j = \frac{\int_0^\pi W_j(\alpha)B(\alpha)p(\alpha)\sin\alpha\, d\alpha}{\int_0^\pi W_j(\alpha)B(\alpha)\sin\alpha\, d\alpha}.$$

Thus, $W_j(\alpha)$ weights the range of true angles that can be reconstructed and accepted in channel j, while $\overline{p}_j$ is the corresponding response-weighted mean of $p(\alpha)$ over that accepted signal-channel response.

The corresponding response-weighted modulation depth is obtained by multiplying $\overline{p}_j$ by the response-weighted Compton analyzing power of the idler analyzer so that

$$\mu_{\Delta\theta,W}(\alpha_j) = \overline{p}_j \frac{\int_0^\pi W_{\Delta\theta}(\theta) E^2(\theta) t_{12}(\theta) \sin\theta \, d\theta}{\int_0^\pi W_{\Delta\theta}(\theta) E^2(\theta) t_{11}(\theta) \sin\theta \, d\theta}.$$

The finite-acceptance result in Eq. (14) is recovered when $W_j(\alpha)$ approaches a narrow response centered on α_j and $W_{\Delta\theta}(\theta)$ equals unity inside $[\theta_-, \theta_+]$ and zero outside. For a finite signal channel, $B(\alpha)$ remains inside the average because it weights the accepted true angles. Nevertheless, its absolute normalization, the total cross section, and the source strength are not required. Finite polar-angle response changes both the signal-side average $\overline{p}_j$ and the response-weighted analyzing power of the idler analyzer, but does not by itself introduce a new azimuthal dependence. A nonuniform azimuthal response can instead distort the cosine form and must be corrected experimentally or incorporated into the detector model.

Azimuthal reconstruction resolution is described separately. Let $\phi_{\rm rec}$ denote the reconstructed idler azimuth, and define the signed azimuthal reconstruction error by

$$\delta\phi = \phi_{\rm rec} - \phi,$$

so that

$$\phi = \phi_{\rm rec} - \delta\phi.$$

Angular differences are understood modulo 2π and represented on the interval $-\pi \leqslant \delta\phi < \pi$. Let $K_j(\delta\phi)$ be the normalized, symmetric azimuthal-resolution kernel for setting j, such that

$$\int_{-\pi}^{\pi} K_j(\delta\phi)\, d\delta\phi = 1, \quad K_j(\delta\phi) = K_j(-\delta\phi).$$

The kernel $K_j(\delta\phi)$ therefore specifies the probability distribution of the signed azimuthal reconstruction error $\delta\phi$.

Let $f_{{\rm bg},j}$ be the fraction of accepted events arising from an azimuthally uniform, uncorrelated background. Such a component can include accidental coincidences and detector dark counts when these are uncorrelated with the reconstructed azimuth. When the response-weighted accepted profile retains the cosine form, the corresponding unit-mean reconstructed relative profile, which generalizes $R_{\Delta\theta}$ in Eq. (13), can be written as

$$R_{\rm rec}(\phi_{\rm rec} \mid \alpha_j, \beta) = \int_{-\pi}^{\pi} K_j(\delta\phi)[1 - (1 - f_{{\rm bg},j})\mu_{\Delta\theta,W}(\alpha_j) \times \cos 2(\beta + \phi_{\rm rec} - \delta\phi)] d\delta\phi.$$

Using

$$\cos 2(\beta + \phi_{\rm rec} - \delta\phi) = \cos 2(\beta + \phi_{\rm rec}) \cos(2\delta\phi) + \sin 2(\beta + \phi_{\rm rec}) \sin(2\delta\phi),$$

together with the symmetry of $K_j(\delta\phi)$, gives

$$\int_{-\pi}^{\pi} K_j(\delta\phi) \sin(2\delta\phi)\, d\delta\phi = 0.$$

The surviving second-harmonic component of the resolution kernel is therefore

$$\kappa_{2,j} = \int_{-\pi}^{\pi} K_j(\delta\phi) \cos(2\delta\phi)\, d\delta\phi.$$

For the resolution responses considered here, we restrict attention to kernels with positive second-harmonic transfer, $\kappa_{2,j} > 0$. The reconstructed relative profile then reduces to

$$R_{\rm rec}(\phi_{\rm rec} \mid \alpha_j, \beta) = 1 - (1 - f_{{\rm bg},j})\kappa_{2,j}\mu_{\Delta\theta,W}(\alpha_j) \times \cos 2(\beta + \phi_{\rm rec}),$$

so that the reconstructed modulation depth is

$$\mu_{\rm rec}(\alpha_j) = (1 - f_{{\rm bg},j})\kappa_{2,j}\mu_{\Delta\theta,W}(\alpha_j).$$

Thus, an azimuthally uniform background reduces the modulation by the factor $1 - f_{{\rm bg},j}$, while finite azimuthal resolution multiplies the surviving second harmonic by the factor $\kappa_{2,j}$.

For a wrapped Gaussian azimuthal-resolution kernel with angular standard deviation $\sigma_{\phi,j}$, expressed in radians, the second-harmonic attenuation factor is

$$\kappa_{2,j} = \exp\big(-2\sigma_{\phi,j}^2\big).$$

The ideal azimuthal-resolution limit corresponds to $\sigma_{\phi,j} \to 0$ and hence $\kappa_{2,j} \to 1$. Here, $f_{{\rm bg},j}$ describes only a residual azimuthally uniform, uncorrelated component. Structured backgrounds, including unresolved multiple scattering, must instead be incorporated through a forward detector simulation.

Any common azimuth-independent multiplicative factor applied to the accepted distribution, including acquisition time, an overall detection efficiency, or the fraction of acquisition time during which the detector is live, cancels from the corresponding modulation ratio. In the absence of an additive background, the absolute source strength likewise cancels. When an additive background is present, however, the source strength is expected to affect the background fraction $f_{{\rm bg},j}$ and hence the reconstructed modulation. Dead time or pileup can bias the recovered modulation if it produces an azimuth-dependent or nonlinear response, for example, through unequal channel occupancies or event migration across the reconstruction cuts. Such effects belong to the apparatus response rather than to the underlying modulation definition.

The effect of an azimuthally uniform, uncorrelated background on the reconstructed modulation separation can also be assessed directly. Define $\Delta\mu_{\rm rec} \equiv \mu_{\rm rec}(\alpha_2) - \mu_{\rm rec}(\alpha_1)$ and $\Delta\mu_{\Delta\theta,W} \equiv \mu_{\Delta\theta,W}(\alpha_2) - \mu_{\Delta\theta,W}(\alpha_1)$. If the same background fraction $f_{\rm bg}$ and resolution factor κ_2 apply to both settings, then

$$\Delta\mu_{\rm rec} = (1 - f_{\rm bg})\kappa_2 \Delta\mu_{\Delta\theta,W},$$

so, provided $\Delta\mu_{\Delta\theta,W} \neq 0$, the two reconstructed modulation levels remain distinct for every $f_{\rm bg} < 1$ and $\kappa_2 > 0$. Even in the deliberately pessimistic case in which the 45° sample is background-free, only the 81.7° sample is contaminated, and the same resolution factor applies to both settings, equality of

the two modulation depths requires

$$f_{\mathrm{bg},2} = 1 - \frac{\mu_{\Delta\theta,W}(45^\circ)}{\mu_{\Delta\theta,W}(81.7^\circ)}.$$

In the ideal narrow-channel limit with full idler polar-angle acceptance used above, this gives

$$f_{\mathrm{bg},2} \simeq 0.539.$$

Here, $N_{\mathrm{bg},2}$ and $N_{\mathrm{sig},2}$ denote the accepted background and true-coincidence counts for setting α_2, respectively. Since

$$f_{\mathrm{bg},2} = \frac{N_{\mathrm{bg},2}}{N_{\mathrm{sig},2} + N_{\mathrm{bg},2}},$$

the corresponding background-to-true-coincidence count ratio is

$$\frac{N_{\mathrm{bg},2}}{N_{\mathrm{sig},2}} = \frac{f_{\mathrm{bg},2}}{1 - f_{\mathrm{bg},2}} \simeq 1.17.$$

This means that approximately 1.17 accepted background events are required for every accepted true-coincidence event in the α_2 sample to eliminate the separation between the two expected modulation levels under this deliberately pessimistic assumption. For general polar-angle response functions under the same background and resolution assumptions, the corresponding threshold is determined by the two response-weighted modulation depths rather than by the nominal angles alone. Statistical distinguishability nevertheless depends on the number of accepted coincidences and is treated separately below.

Modern annihilation-photon measurements implement these apparatus-dependent corrections through event mixing and detector-response simulations [12–14]. In particular, Bordes *et al.* corrected the measured azimuthal acceptance using mixed uncorrelated events and used a GEANT4-based model to incorporate detector acceptance, reconstruction resolution, and multiple-scattering contributions [14]. The agreement between the reconstructed data and the simulation demonstrates that a forward detector model can account for the dominant apparatus effects without modifying the underlying $\cos 2\phi$ correlation law. Consistent with the idealized scope of the present analysis, the quantitative baseline below uses the narrow signal-channel limit for W_j, the ideal full-polar-angle-acceptance limit for $W_{\Delta\theta}$, $f_{\mathrm{bg},j} = 0$, and $\kappa_{2,j} = 1$. The corresponding response functions and parameters for a specific implementation would be obtained from detector simulation and calibration data.

III. TIMING AND CONTROL MODEL

This section gives the coincidence-conditioned Stokes vector in Eq. (4b) an operational meaning by specifying how the two signal-arm selections are applied in time and how the corresponding idler events are recorded. The timing construction is first stated for the ideal response used for the baseline results in Sec. II. Finite acceptance, angular resolution, and azimuthally uniform residual backgrounds enter through the retained coincidence rate and through the reconstructed modulation $\mu_{\mathrm{rec}}(\alpha_j)$ defined there. Structured backgrounds and multiple-scattering contributions require the corresponding forward detector model.

Two distinct timescales are required. The quantity $\Delta\tau$ denotes the acquisition interval over which events are accumulated for one fixed signal-arm setting. In contrast, $d\tau$ denotes the half-width of the symmetric coincidence time window used to decide whether a signal event and an idler event are consistent with originating from the same annihilation pair. Thus, $d\tau$ governs pair identification, whereas $\Delta\tau$ governs the number of retained coincidences available for estimating the modulation in a given interval.

The signal control station selects between the two fixed channel settings $\alpha_1 = 45^\circ$ and $\alpha_2 = 81.7^\circ$. Let $b_k \in \{0, 1\}$ denote the prescribed binary setting in the kth acquisition interval, with $b_k = 0$ selecting α_1 and $b_k = 1$ selecting α_2. Writing the prescribed binary control sequence as $\mathbf{b}$, the illustrative five-interval sequence shown in Fig. 4 is therefore

$$\mathbf{b} = (b_0, b_1, b_2, b_3, b_4) = (0, 0, 0, 0, 1).$$

The sequence is used only to illustrate the timing and classification procedure. The physical observable is the coincidence-conditioned modulation associated with the active signal-arm setting.

Operationally, selection of the active channel in the kth interval is controlled by a channel-select gating pulse (CSGP). Let $G_k(t)$ denote the corresponding gate function, with $G_k(t) = 1$ only during the active part of that interval. The corresponding channel-control functions for the two channels are

$$H_1(t) = G_k(t)(1 - b_k), \quad H_2(t) = G_k(t)b_k.$$

When $G_k(t) = 1$, exactly one of $H_1(t)$ or $H_2(t)$ is enabled according to b_k. When $G_k(t) = 0$, both channels are disabled. This logic-level description shows how the prescribed sequence of signal settings can be implemented without mechanically reorienting a single collimator.

The signal-arm detector records and time-tags photons accepted through the enabled channel, producing the time-tag list $\{\tau_{s,n}\}$, where n indexes accepted signal events. The idler analysis station independently records the continuous idler stream, producing the time-tag list $\{\tau_{i,m}\}$, where m indexes recorded idler events. Each idler event m is also assigned the reconstructed Compton-scattering angles $(\theta_{i,m}, \phi_{i,m})$. Before coincidence selection, this idler stream represents the unconditional idler ensemble and therefore contains no local polarization modulation associated with the prescribed signal-control sequence. The modulation predicted in Sec. II appears only after the idler events are conditioned on accepted signal-arm detections.

For a fixed setting α_j and a specified idler acceptance $\Delta\theta$, let $R_{\mathrm{coinc},j}$ denote the total rate of coincidences retained after application of the coincidence criterion and event-selection cuts. This rate contains the retained true-coincidence contribution $R_{\mathrm{sig},j}$ together with any accepted background contribution $R_{\mathrm{bg},j}$, so that

$$R_{\mathrm{coinc},j} = R_{\mathrm{sig},j} + R_{\mathrm{bg},j}.$$

When accidental coincidences, denoted by $R_{\mathrm{acc},j}$, dominate the uncorrelated background, $R_{\mathrm{bg},j} \simeq R_{\mathrm{acc},j}$. These accidental events contribute to the retained coincidence stream and therefore to the total coincidence rate $R_{\mathrm{coinc},j}$ that determines how rapidly events accumulate. Let N_k denote the number of

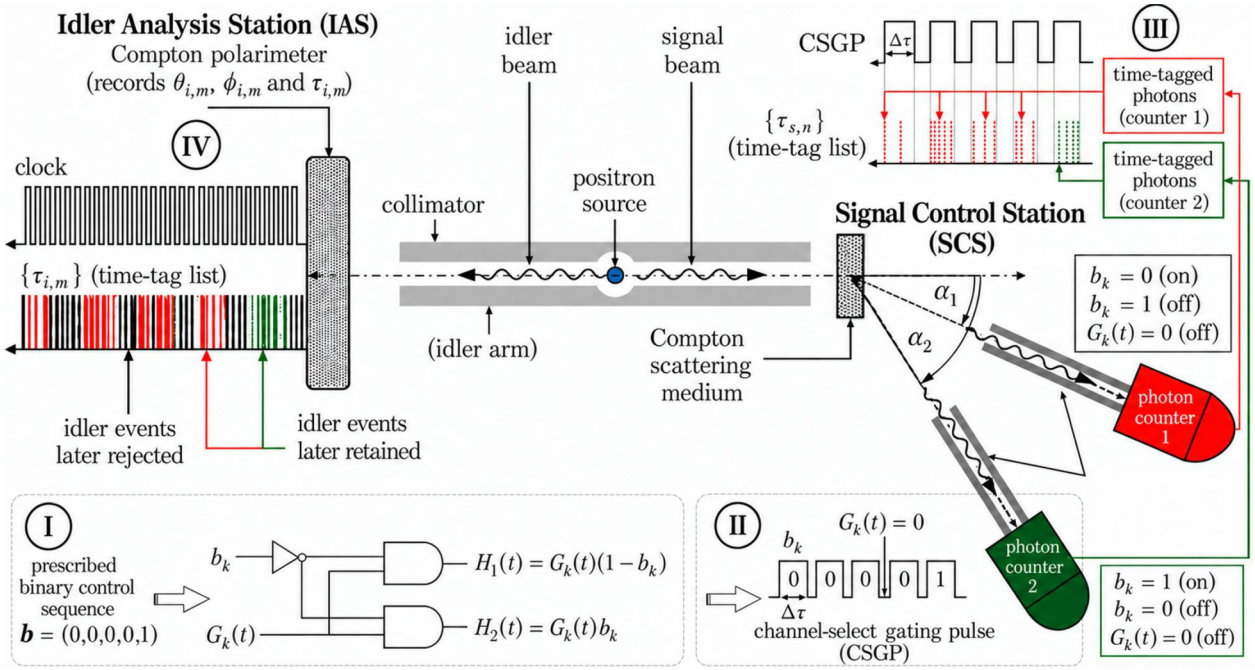


FIG. 4. Idealized timing and control scheme. An electron-positron annihilation source emits back-to-back 511 keV photon pairs toward the signal control station (SCS) and idler analysis station (IAS). Panel (I) shows the prescribed binary control sequence **b**, with $b_k \in \{0, 1\}$ denoting its value in acquisition interval k, and the logic defining the channel-control functions $H_1(t) = G_k(t)(1 - b_k)$ and $H_2(t) = G_k(t)b_k$. Panel (II) shows the CSGP, with $G_k(t)$ denoting the gate function for acquisition interval k of duration $\Delta\tau$, together with the signal-side Compton-scattering geometry and the two fixed channels centered on α_1 and α_2. For $G_k(t) = 1$, the value $b_k = 0$ enables the channel centered on α_1, whereas $b_k = 1$ enables the channel centered on α_2. When $G_k(t) = 0$, both channels are disabled. Panel (III) shows the accepted signal events and their time-tag list $\{\tau_{s,n}\}$, where n indexes accepted signal events. Panel (IV) shows the continuously recorded idler stream and its time-tag list $\{\tau_{i,m}\}$, where m indexes recorded idler events, with each event also assigned reconstructed angles $(\theta_{i,m}, \phi_{i,m})$. The colored idler events illustrate those subsequently retained by the coincidence filtering shown in Fig. 5, while the remaining recorded idler events are rejected.

retained coincidences in acquisition interval k. For an interval generated with setting α_j, its expected value is

$$\mathbb{E}[N_k] \simeq \Delta\tau\, R_{\mathrm{coinc},j}.$$

Here, $\mathbb{E}$ denotes statistical expectation. Because $R_{\mathrm{coinc},j}$ may differ between the two signal settings, a common acquisition duration $\Delta\tau$ need not produce the same expected retained count for both. We therefore assume that $\Delta\tau$ is chosen sufficiently long to satisfy the required event-count criterion for either prescribed setting. The corresponding condition is derived in Sec. IV.

The source-side production rate of 511 keV annihilation-photon pairs and the retained coincidence rate $R_{\mathrm{coinc},j}$ are distinct quantities. Source activity sets the underlying decay and annihilation rate, subject to the positron-emission and annihilation-channel branching fractions. The retained rate is generally much smaller because it additionally includes geometric acceptance, the required Compton interactions, detection efficiency, reconstruction, coincidence selection, and event-selection cuts. Although the absolute source strength cancels from the ideal relative modulation $\mu_{\Delta\theta}$, it contributes to $R_{\mathrm{coinc},j}$ and therefore affects the mean-count acquisition time associated with a specified classification criterion. In the presence of additive background, increasing the source activity can also alter the background fraction and hence the reconstructed modulation. The required event count and its dependence on the selected signal-arm settings are derived in Sec. IV.

IV. COINCIDENCE FILTERING AND MODULATION CLASSIFICATION

The postselection and classification procedure is summarized in Fig. 5. It specifies how the signal-side time-tag list $\{\tau_{s,n}\}$ introduced in Sec. III is used to construct the coincidence-conditioned idler ensemble and recover the sequence of signal-arm settings without requiring a particular detector architecture.

Panel (I) represents synchronization of the idler clock with the channel-select gating pulse and partitioning of the continuously recorded idler stream into acquisition intervals. The signal control station and idler analysis station are assumed to share a common time base up to a fixed offset $\delta\tau_0$ that is known or calibrated. Each idler event is recorded as $(\tau_{i,m}, \theta_{i,m}, \phi_{i,m})$, while each accepted signal event contributes a time tag $\tau_{s,n}$. Each active acquisition interval has duration $\Delta\tau$. Events recorded while $G_k(t) = 0$ are excluded from the active intervals.

Panel (II) represents coincidence identification. A signal event with time tag $\tau_{s,n}$ and an idler event with time tag $\tau_{i,m}$ are treated as belonging to the same annihilation pair when

$$|\tau_{i,m} - \tau_{s,n} - \delta\tau_0| \leqslant d\tau.$$

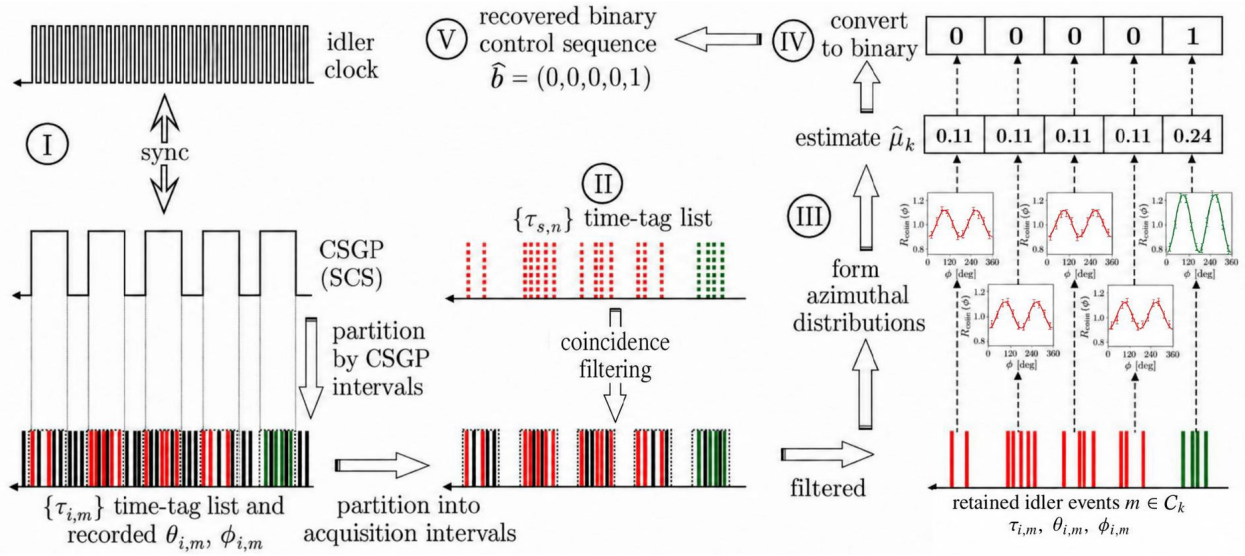


FIG. 5. Idealized coincidence-filtering and modulation-classification scheme. Panel (I) shows synchronization of the idler clock with the CSGP and partition of the continuously recorded idler stream $\{\tau_{i,m}\}$ into acquisition intervals of duration $\Delta\tau$. Panel (II) shows coincidence filtering using the signal-side time-tag list $\{\tau_{s,n}\}$. For acquisition interval k, let $\mathcal{C}_k$ denote the set of indices m of idler events in that interval for which $|\tau_{i,m} - \tau_{s,n} - \delta\tau_0| \leqslant d\tau$ for at least one accepted signal event n, where $\delta\tau_0$ is the known or calibrated fixed timing offset between the two stations and $d\tau$ is the half-width of the symmetric coincidence time window. Panel (III) shows the retained idler events, indexed by $m \in \mathcal{C}_k$, with recorded quantities $(\tau_{i,m}, \theta_{i,m}, \phi_{i,m})$, and the estimation of the corresponding azimuthal modulation depth. In the idealized analysis considered here, the full idler polar-angle acceptance $\Delta\theta = [0, \pi]$ is used, and the retained azimuthal sample is used to obtain the modulation estimator $\widehat{\mu}_k$ for interval k. Representative schematic points with illustrative statistical uncertainties are shown together with schematic modulation curves to indicate the finite-sample estimation step. The points and error bars do not represent experimental data or results of an independent numerical simulation. Panel (IV) shows classification of $\widehat{\mu}_k$ relative to the reference levels $\mu_{[0,\pi]}(\alpha_1)$ and $\mu_{[0,\pi]}(\alpha_2)$ to obtain $\widehat{b}_k$. Panel (V) shows the recovered binary control sequence $\widehat{\mathbf{b}}$.

For acquisition interval k, let $\mathcal{C}_k$ denote the set of indices m of idler events in that interval for which this criterion is satisfied for at least one accepted signal event n. The retained idler events are therefore indexed by $m \in \mathcal{C}_k$, and the retained-coincidence count introduced in Sec. III is $N_k = |\mathcal{C}_k|$.

For accidental pairings between statistically independent signal-arm and idler-arm singles entering the coincidence test, let $R_{s,j}$ and R_i denote the corresponding mean singles rates, respectively. The accidental-coincidence rate admitted by this symmetric coincidence window is, to leading order,

$$R_{\mathrm{acc},j} \simeq 2d\tau\, R_{s,j} R_i. \tag{15}$$

The factor $2d\tau$ is the total width of the accepted coincidence interval. This estimate assumes stationary singles rates over the acquisition interval, statistically independent accidental pairings, sufficiently low singles rates that multiple detections within one coincidence window are negligible, and negligible distortions from dead time or pileup. Using Eq. (15), if accidental coincidences are azimuthally uniform and constitute the dominant uncorrelated background for setting j, their contribution to the background fraction is approximately

$$f_{\mathrm{bg},j} \simeq \frac{R_{\mathrm{acc},j}}{R_{\mathrm{sig},j} + R_{\mathrm{acc},j}},$$

where $R_{\mathrm{sig},j}$ is the retained true-coincidence rate. The corresponding reconstructed modulation is

$$\mu_{\mathrm{rec}}(\alpha_j) = (1 - f_{\mathrm{bg},j})\kappa_{2,j}\mu_{\Delta\theta,W}(\alpha_j),$$

as derived in Sec. II. Additional azimuthally uniform, uncorrelated background sources can be included in $f_{\mathrm{bg},j}$. Azimuthally structured backgrounds must instead be incorporated through a forward detector simulation, as discussed there.

The retained idler events indexed by $m \in \mathcal{C}_k$ define the coincidence-conditioned ensemble in acquisition interval k. Panel (III) represents construction of the azimuthal sample from this retained ensemble. The idealized baseline considered here uses the full idler polar-angle acceptance

$$\Delta\theta = [0, \pi].$$

No additional polar-angle rejection is therefore applied to the retained coincidences in this baseline. The general finite-acceptance and detector-response extensions are given in Sec. II. For the full-polar-angle baseline, the relative azimuthal profile is

$$R_{[0,\pi]}(\phi \mid \alpha_j, \beta) = 1 - \mu_{[0,\pi]}(\alpha_j)\cos 2(\beta + \phi).$$

Panel (III) schematically represents estimating the modulation depth from the retained azimuthal distribution in each interval. The representative points and error bars illustrate the finite-sample estimation step and are not independent experimental or numerical-simulation results. For the quantitative statistical treatment, we use the unbiased moment estimator defined explicitly below.

For the ideal narrow-signal-channel, full-polar-angle baseline used in Fig. 3, the two reference levels are

$$\mu_1 \equiv \mu_{[0,\pi]}(45^\circ) \simeq 0.109\,62,$$
$$\mu_2 \equiv \mu_{[0,\pi]}(81.7^\circ) \simeq 0.237\,58,$$

with separation

$$\Delta\mu \equiv \mu_2 - \mu_1 \simeq 0.127\,95.$$

Thus, for the prescribed pair $\alpha_1 = 45^\circ$ and $\alpha_2 = 81.7^\circ$, $\Delta\mu$ denotes the ideal full-polar-angle separation $\Delta\mu_{[0,\pi]}$ defined in Sec. II. Its dependence on a variable choice of α_1 is considered below.

Panel (IV) implements binary classification by comparing the estimated modulation $\widehat{\mu}_k$ with the midpoint

$$\mu_* \equiv \frac{\mu_1 + \mu_2}{2} \simeq 0.173\,60.$$

For the ideal baseline, we adopt the midpoint rule in which $\widehat{\mu}_k < \mu_*$ is assigned $\widehat{b}_k = 0$, corresponding to the α_1 setting, and $\widehat{\mu}_k \geqslant \mu_*$ is assigned $\widehat{b}_k = 1$, corresponding to the α_2 setting. This midpoint classifier provides a simple reference decision rule. With unequal variances, unequal prior probabilities, or detector-dependent response, the optimal threshold need not coincide with the midpoint and should instead be obtained from the corresponding likelihood model. For a specified detector response that preserves the cosine form, the same midpoint construction may be applied using the reconstructed reference levels $\mu_{\mathrm{rec}}(\alpha_1)$ and $\mu_{\mathrm{rec}}(\alpha_2)$, with the class assignment determined by their ordering.

The finite coincidence count determines how reliably the two modulation levels can be separated. For the ideal narrow-signal-channel, full-polar-angle baseline with known β, the unit-mean relative profile in Eq. (13), evaluated for $\Delta\theta = [0, \pi]$, gives the normalized azimuthal probability density

$$f_\phi(\phi \mid \mu_j, \beta) = \frac{1}{2\pi}[1 - \mu_j \cos 2(\beta + \phi)],$$

where $\mu_j = \mu_{[0,\pi]}(\alpha_j)$ for $j = 1, 2$.

Assuming the retained idler events indexed by $m \in \mathcal{C}_k$ are independent samples from the distribution above, an unbiased moment estimator of the modulation in interval k is

$$\widehat{\mu}_k = -\frac{2}{N_k} \sum_{m \in \mathcal{C}_k} \cos 2(\beta + \phi_{i,m}). \tag{16}$$

The estimator in Eq. (16) has variance

$$\mathrm{Var}(\widehat{\mu}_k \mid \mu_j, N_k) = \frac{2 - \mu_j^2}{N_k}.$$

Accordingly, under the Gaussian approximation, the conditional distribution of the estimator is

$$\widehat{\mu}_k \mid (\mu_j, N_k) \sim \mathcal{N}\left(\mu_j, \frac{2 - \mu_j^2}{N_k}\right).$$

Here, $\mathcal{N}$ denotes the normal distribution, with its first and second arguments giving the mean and variance, respectively.

Let Φ denote the cumulative distribution function of the standard normal distribution. For the midpoint classifier, let $P_{\mathrm{err},j}(N_k)$ denote the class-conditional probability of assigning an interval generated by setting α_j to the wrong setting. It is given by

$$P_{\mathrm{err},j}(N_k) = 1 - \Phi\left[\frac{\Delta\mu}{2}\sqrt{\frac{N_k}{2 - \mu_j^2}}\right], \quad j = 1, 2. \tag{17}$$

For equal prior probabilities, let $P_{\mathrm{err}}(N_k)$ denote the corresponding mean classification-error probability. Using Eq. (17),

$$P_{\mathrm{err}}(N_k) = \tfrac{1}{2}[P_{\mathrm{err},1}(N_k) + P_{\mathrm{err},2}(N_k)].$$

To define the conservative minimum event count $N_{\mathrm{min},j}$ for setting α_j, we require a two-sided 95% Gaussian interval about either expected modulation level to remain on its own side of the midpoint. This gives

$$1.96\sqrt{\frac{2 - \mu_j^2}{N_{\mathrm{min},j}}} \leqslant \frac{\Delta\mu}{2}. \tag{18}$$

This condition places the classification threshold at least 1.96 standard deviations from either expected level. It therefore corresponds to a one-sided class-conditional misclassification probability no greater than

$$1 - \Phi(1.96) \simeq 0.025$$

under the Gaussian approximation. The criterion is consequently more conservative than requiring a 95% probability of correct classification for each setting.

Solving Eq. (18) gives

$$N_{\mathrm{min},j} \geqslant \left(\frac{2 \times 1.96}{\Delta\mu}\right)^2 (2 - \mu_j^2).$$

Evaluating the equality limits for the two prescribed baseline reference levels gives

$$N_{\mathrm{min},1} \simeq 1.87 \times 10^3, \quad N_{\mathrm{min},2} \simeq 1.82 \times 10^3.$$

Defining $N_{\mathrm{min}} \equiv \max_{j=1,2} N_{\mathrm{min},j}$ as the common ideal event requirement, the full-polar-angle calculation gives $N_{\mathrm{min}} \simeq 1.87 \times 10^3$ retained coincidences per active acquisition interval, which we round to approximately 2×10^3 for the conservative event requirement used here.

The numerical event requirement above corresponds to the particular choice $\alpha_1 = 45^\circ$ and $\alpha_2 = 81.7^\circ$. To generalize this result, we keep $\alpha_2 = 81.7^\circ$ fixed and allow α_1 to vary over the lower-angle range $0 \leqslant \alpha_1 \leqslant 80^\circ$ considered in Fig. 6. The corresponding ideal full-polar-angle modulation separation is

$$\Delta\mu(\alpha_1) \equiv \mu_2 - \mu_{[0,\pi]}(\alpha_1),$$

where $\mu_2 = \mu_{[0,\pi]}(81.7^\circ)$. Over the displayed interval, $\mu_{[0,\pi]}(\alpha_1) < \mu_2$, so that $\Delta\mu(\alpha_1) > 0$. The midpoint classification threshold is then

$$\mu_*(\alpha_1) = \frac{\mu_{[0,\pi]}(\alpha_1) + \mu_2}{2}.$$

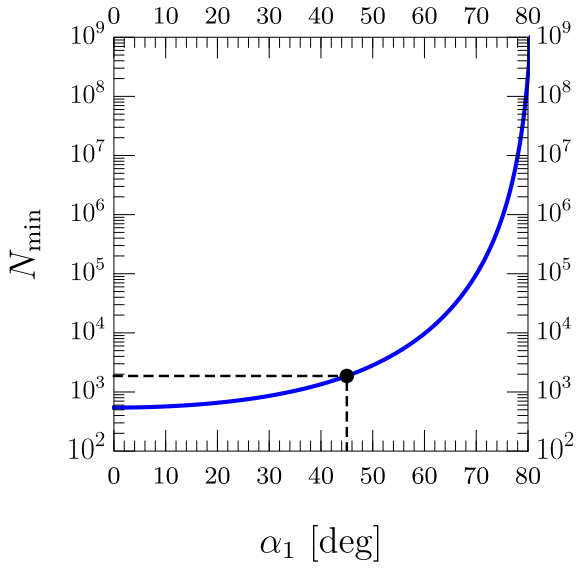


FIG. 6. Conservative minimum retained-coincidence requirement $N_{\min}(\alpha_1)$ for discriminating a variable signal-arm setting α_1 from the fixed reference setting $\alpha_2 = 81.7^\circ$ under the ideal narrow-signal-channel, full-polar-angle model. For each α_1, $N_{\min}(\alpha_1) = \max\{N_{\min,1}(\alpha_1), N_{\min,2}(\alpha_1)\}$ is obtained from the two-sided 95% midpoint separation criterion in Eq. (18). The two class-specific requirements are nearly coincident over the displayed interval, so only their conservative envelope is shown. The vertical axis is logarithmic. The point and dashed guide lines mark $\alpha_1 = 45^\circ$, for which $N_{\min} \simeq 1.87 \times 10^3$. The plotted range terminates at $\alpha_1 = 80^\circ$ to remain on the lower-angle branch below the maximum of the Compton analyzing power. The rapid increase in $N_{\min}$ reflects the dominant $[\Delta\mu(\alpha_1)]^{-2}$ dependence of the required count as the two modulation levels approach one another.

The equality limits of Eq. (18) define the two class-specific event-count thresholds

$$N_{\min,1}(\alpha_1) = \left[\frac{2 \times 1.96}{\Delta\mu(\alpha_1)}\right]^2 \left[2 - \mu^2_{[0,\pi]}(\alpha_1)\right],$$

$$N_{\min,2}(\alpha_1) = \left[\frac{2 \times 1.96}{\Delta\mu(\alpha_1)}\right]^2 \left[2 - \mu_2^2\right].$$

The corresponding conservative common requirement is

$$N_{\min}(\alpha_1) \equiv \max\{N_{\min,1}(\alpha_1), N_{\min,2}(\alpha_1)\}.$$

Figure 6 shows $N_{\min}(\alpha_1)$ for the fixed reference setting $\alpha_2 = 81.7^\circ$. The two class-specific requirements are nearly coincident over the displayed interval, so only their conservative envelope is shown. The marked point at $\alpha_1 = 45^\circ$ recovers the value used above, $N_{\min} \simeq 1.87 \times 10^3$. Decreasing α_1 increases the modulation separation and reduces the required coincidence count, reaching $N_{\min} \simeq 5.45 \times 10^2$ at $\alpha_1 = 0^\circ$. Conversely, as α_1 increases across the displayed interval, $\Delta\mu(\alpha_1)$ decreases and the required count rises rapidly according to the dominant $[\Delta\mu(\alpha_1)]^{-2}$ dependence.

The end point $\alpha_1 = 0^\circ$ should be understood as a formal limit of the idealized angular model rather than as a practical detector operating point. At exact forward scattering, the Compton energy transfer vanishes, so such an event does not provide a practical signal-arm scattering trigger. The reduction in $N_{\min}$ at smaller α_1 does not by itself identify an experimentally optimal signal setting. The result isolates the statistical requirement associated with modulation separation, whereas the detector-dependent mean-count acquisition time also depends on the retained coincidence rates and reconstructed modulation levels through $R_{\mathrm{coinc},j}$ and $\mu_{\mathrm{rec},j}$, as considered below.

The preceding event-count criterion applies directly to the ideal modulation levels. For a specified detector response that preserves the cosine form, the same statistical construction applies after replacing the ideal modulation levels by their reconstructed counterparts. Define

$$\mu_{\mathrm{rec},j} \equiv \mu_{\mathrm{rec}}(\alpha_j).$$

The reconstructed modulation separation defined in Sec. II can then be written as

$$\Delta\mu_{\mathrm{rec}} = \mu_{\mathrm{rec},2} - \mu_{\mathrm{rec},1}.$$

For a variable choice of α_1 with $\alpha_2 = 81.7^\circ$ fixed, the corresponding reconstructed separation may likewise be written as $\Delta\mu_{\mathrm{rec}}(\alpha_1) = \mu_{\mathrm{rec}}(81.7^\circ) - \mu_{\mathrm{rec}}(\alpha_1)$. For compactness, the explicit dependence on the selected pair of signal-arm settings is suppressed in the notation below. Let $N^{\mathrm{rec}}_{\min,j}$ denote the corresponding minimum event count for the reconstructed reference levels. Applying the same conservative midpoint criterion gives

$$N^{\mathrm{rec}}_{\min,j} \geqslant \left(\frac{2 \times 1.96}{|\Delta\mu_{\mathrm{rec}}|}\right)^2 (2 - \mu^2_{\mathrm{rec},j}),$$

provided the reconstructed modulation levels remain distinct. The dominant dependence on their separation therefore scales as $|\Delta\mu_{\mathrm{rec}}|^{-2}$.

Combining this event requirement with the total retained coincidence rate defined in Sec. III gives the acquisition duration for which the expected retained count reaches the required event count,

$$\Delta\tau_{\min,j} = \frac{N^{\mathrm{rec}}_{\min,j}}{R_{\mathrm{coinc},j}}. \tag{19}$$

In the ideal background-free, perfect-resolution limit with a narrow signal channel and full idler polar-angle acceptance, $\mu_{\mathrm{rec},j} \to \mu_j$, $N^{\mathrm{rec}}_{\min,j} \to N_{\min,j}$, and $R_{\mathrm{coinc},j} \to R_{\mathrm{sig},j}$. Equation (19) then reduces to the corresponding ideal mean-count acquisition time. For the common acquisition duration assumed in Sec. III, the corresponding mean-count condition is

$$\Delta\tau \geqslant \max_{j=1,2} \Delta\tau_{\min,j}.$$

An order-of-magnitude comparison with existing double-Compton measurements provides an experimental scale for these quantities. The quantum-enabled PET (QEPET) measurements of Kim *et al.* used initial source activities of 6 and 28 MBq and obtained retained double-Compton event rates of 0.105 and 0.690 s^{-1}, respectively [13]. These measurements therefore establish a retained-event rate scale of order 10^{-1} to 10^{0} s^{-1} for that detector geometry and event-selection procedure. The corresponding source-side decay rates are of order 10^6–10^7 s^{-1}, and the source-side two-photon annihilation-pair production rate has the same order

of magnitude up to the positron-emission and annihilation-channel branching fractions. Combining the experimentally demonstrated retained-event rate scale with the ideal requirement $N_{\min} \simeq 1.87 \times 10^3$ for the prescribed pair $\alpha_1 = 45^\circ$ and $\alpha_2 = 81.7^\circ$, rounded to approximately 2×10^3 events for the criterion used here, gives an acquisition timescale of order 10^3–10^4 s, corresponding to tens of minutes to several hours.

These values are order-of-magnitude experimental benchmarks rather than predictions for the idealized geometry considered here. The detector-specific mean-count acquisition time must instead be evaluated from Eq. (19) using the reconstructed requirement $N^{\mathrm{rec}}_{\min,j}$ and the retained coincidence rate $R_{\mathrm{coinc},j}$. Both quantities depend on the experimental response. In particular, increasing source activity can raise the retained event rate while also increasing accidental coincidences and thereby reducing the magnitude of the separation $|\Delta\mu_{\mathrm{rec}}|$. A realistic acquisition-time estimate therefore requires the source activity, geometry, accepted solid angle, detector efficiency, angular response, event-selection cuts, live time, background, and coincidence window of the particular implementation.

Panel (V) represents the final recovery of the prescribed binary control sequence from the classified acquisition intervals. The recovered sequence is denoted by $\widehat{\mathbf{b}}$, whose entries are the classified values $\widehat{b}_k$. For the illustrative five-interval example in Figs. 4 and 5,

$$\widehat{\mathbf{b}} = (\widehat{b}_0, \widehat{b}_1, \widehat{b}_2, \widehat{b}_3, \widehat{b}_4) = (0, 0, 0, 0, 1).$$

This sequence is only a compact example of the procedure. No practical communication performance or security claim is implied.

V. CONCLUSION

The present work builds on the Bell-orbit polarization-symmetry result of Ref. [24] by giving its predicted coincidence-conditioned response an explicit timing, postselection, and modulation-classification procedure. The observable carried through the analysis is the relative azimuthal modulation depth $\mu_{\Delta\theta}$ defined in Sec. II. For the ideal narrow-signal-channel, full-polar-angle baseline considered here, the prescribed signal settings $\alpha_1 = 45^\circ$ and $\alpha_2 = 81.7^\circ$ give $\mu_{[0,\pi]} \simeq 0.109\,62$ and $0.237\,58$, respectively.

The timing model separates the coincidence-window half-width $d\tau$, which governs identification of candidate photon pairs, from the acquisition interval $\Delta\tau$, over which enough retained coincidences are accumulated to estimate one modulation level. Coincidence postselection then defines the idler ensemble associated with each signal setting, and its azimuthal modulation depth is estimated and classified relative to the two predicted reference levels. For the prescribed pair $\alpha_1 = 45^\circ$ and $\alpha_2 = 81.7^\circ$, the ideal narrow-signal-channel, full-polar-angle finite-statistics analysis gives an event requirement of order 2×10^3 retained coincidences per interval for the conservative two-sided 95% separation criterion used here. For the family of signal settings considered here, the required count decreases as the modulation separation increases and rises rapidly as the two modulation levels approach one another. For a specified detector response that preserves the cosine form, the required count is instead $N^{\mathrm{rec}}_{\min,j}$, and the corresponding detector-dependent mean-count acquisition time is $\Delta\tau_{\min,j} = N^{\mathrm{rec}}_{\min,j}/R_{\mathrm{coinc},j}$. The experimental benchmark discussed in Sec. IV places retained double-Compton rates at approximately 10^{-1} to 10^{0} s^{-1} for the QEPET measurements considered there, giving an acquisition timescale of order 10^3–10^4 s when combined with the ideal event requirement for the prescribed $\alpha_1 = 45^\circ$ and $\alpha_2 = 81.7^\circ$ pair.

The ideal modulation levels are modified in a physical apparatus by finite signal-channel width, idler polar-angle acceptance, angular reconstruction, and residual backgrounds. These effects are represented, within the response model of Sec. II, by the response-weighted modulation $\mu_{\Delta\theta,W}$ and the reconstructed modulation μ_{rec}. Structured backgrounds and multiple-scattering contributions require explicit calibration or forward detector simulation. A common azimuth-independent multiplicative efficiency factor does not alter the relative modulation itself, but it changes the retained coincidence rate and hence the mean-count acquisition time. Source activity likewise enters the retained coincidence rate, while in the presence of additive background it can also change the background fraction and therefore the reconstructed modulation.

The framework should not be interpreted as a Bell-inequality test or as a standalone entanglement-verification procedure. The recovered $\cos 2\phi$ modulation is a model-dependent Compton-polarimetry observable whose interpretation relies on the specified Bell-state and detector-response model. The two-setting implementation therefore tests consistency with a prescribed Bell-state baseline. Identifying an unknown state as Bell-equivalent would require a more complete angular reconstruction together with statistical comparison against separable and partially entangled alternatives.

A natural extension is to insert a controlled interaction on the idler path before the final polarimeter and propagate its effect through the same response and classification framework. Changes in μ_{rec}, the retained coincidence rate, or the full angular profile could then be compared with an explicit channel model. In that form, the present construction provides a baseline for future studies of Bell-orbit symmetry, disturbance, and high-energy polarization-sensitive measurements using time-tagged Compton data.

ACKNOWLEDGMENTS

This work was supported by the Japan Society for the Promotion of Science Grants-in-Aid for Scientific Research under Grants No. 22H05022 and No. 25K01688. This work was also supported in part by JST COI-NEXT under Grant No. JPMJPF2221, MEXT Q-LEAP under Grant No. JPMXS0118067246, and the UTokyo Quantum Initiative. T.S. also acknowledges support from Project No. JPNP20017 commissioned by the New Energy and Industrial Technology Development Organization (NEDO). OpenAI's ChatGPT (GPT-5 and GPT-6) was used as an auxiliary tool during the preparation and revision of this manuscript. Its contributions included assistance with selected mathematical derivations, equations, and scientific arguments, particularly in Secs. II C

and IV, as well as minor cosmetic refinements to Figs. 1, 2, 4, and 5, which were originally constructed independently, without modification of their underlying scientific content. The authors directed the AI-assisted work, reviewed and evaluated its mathematical and scientific outputs, and retain full responsibility for the accuracy, physical consistency, and conclusions of the manuscript. Figures 3 and 6 were generated independently without AI-assisted graphical modification. ChatGPT also assisted with language refinement and manuscript presentation.

DATA AVAILABILITY

The data that support the findings of this article are not publicly available. The data are available from the authors upon reasonable request.

[1] C. Antonelli, M. Shtaif, and M. Brodsky, Sudden death of entanglement induced by polarization mode dispersion, Phys. Rev. Lett. **106**, 080404 (2011).

[2] G. H. Aguilar, A. Valdés-Hernández, L. Davidovich, S. P. Walborn, and P. H. S. Ribeiro, Experimental entanglement redistribution under decoherence channels, Phys. Rev. Lett. **113**, 240501 (2014).

[3] C. H. Bennett, D. P. DiVincenzo, P. W. Shor, J. A. Smolin, B. M. Terhal, and W. K. Wootters, Remote state preparation, Phys. Rev. Lett. **87**, 077902 (2001).

[4] N. A. Peters, J. T. Barreiro, M. E. Goggin, T.-C. Wei, and P. G. Kwiat, Remote state preparation: Arbitrary remote control of photon polarization, Phys. Rev. Lett. **94**, 150502 (2005).

[5] C. S. Wu and I. Shaknov, The angular correlation of scattered annihilation radiation, Phys. Rev. **77**, 136 (1950).

[6] H. Langhoff, Die Linearpolarisation der Vernichtungsstrahlung von Positronen, Z. Phys. **160**, 186 (1960).

[7] L. R. Kasday, J. Ullman, and C. S. Wu, Angular correlation of Compton-scattered annihilation photons and hidden variables, Nuov. Cim. B **25**, 633 (1975).

[8] G. Bertolini, E. Diana, and A. Scotti, Correlation of annihilation γ-ray polarization, Nuov. Cim. B **63**, 651 (1981).

[9] M. Makek, D. Bosnar, L. Pavelić, P. Šenjug, and P. Žugec, Single-layer Compton detectors for measurement of polarization correlations of annihilation quanta, Nucl. Instrum. Methods Phys. Res., Sect. A **958**, 162835 (2020).

[10] D. Abdurashitov, A. Baranov, D. Borisenko, F. Guber, A. Ivashkin, S. Morozov, S. Musin, A. Strizhak, I. Tkachev, V. Volkov, and B. Zhuikov, Setup of Compton polarimeters for measuring entangled annihilation photons, J. Instrum. **17**, P03010 (2022).

[11] F. Lei, A. J. Dean, and G. L. Hills, Compton polarimetry in gamma-ray astronomy, Space Sci. Rev. **82**, 309 (1997).

[12] D. P. Watts, J. Bordes, J. R. Brown, A. Cherlin, R. Newton, J. Allison, M. Bashkanov, N. Efthimiou, and N. A. Zachariou, Photon quantum entanglement in the MeV regime and its application in PET imaging, Nat. Commun. **12**, 2646 (2021).

[13] D. Kim, A. N. Rachman, U. Taisei, M. Uenomachi, K. Shimazoe, and H. Takahashi, Background reduction in PET by double Compton scattering of quantum entangled annihilation photons, J. Instrum. **18**, P07007 (2023).

[14] J. Bordes, J. R. Brown, D. P. Watts, M. Bashkanov, K. Gibson, R. Newton, and N. Zachariou, First detailed study of the quantum decoherence of entangled gamma photons, Phys. Rev. Lett. **133**, 132502 (2024).

[15] I. Tkachev, S. Musin, D. Abdurashitov, A. Baranov, F. Guber, A. Ivashkin, and A. Strizhak, Measuring the evolution of entanglement in Compton scattering, Sci. Rep. **15**, 6064 (2025).

[16] D. Bohm and Y. Aharonov, Discussion of experimental proof for the paradox of Einstein, Rosen, and Podolsky, Phys. Rev. **108**, 1070 (1957).

[17] P. Caradonna and K. Shimazoe, Entanglement, steering, and separability in Compton-scattered annihilation photons, Phys. Rev. A **112**, 032413 (2025).

[18] Z. A. Ravari and Z. Riazi, Quantifying quantum correlations in annihilation photon pairs under Compton scattering, Eur. Phys. J. Plus **141**, 728 (2026).

[19] B. C. Hiesmayr and P. Moskal, Witnessing entanglement in Compton scattering processes via mutually unbiased bases, Sci. Rep. **9**, 8166 (2019).

[20] P. Caradonna, I. D'Amico, D. G. Jenkins, and D. P. Watts, Stokes-parameter representation for Compton scattering of entangled and classically correlated two-photon systems, Phys. Rev. A **109**, 033719 (2024).

[21] J. Clarke, P. Asenov, J. Smeets, J.-S. Wang, D. B. Cassidy, and A. Serafini, Bell test of photons from electron-positron annihilation via POVM-based Compton polarimetry, arXiv:2604.25034.

[22] J. Clarke and A. Serafini (private communication).

[23] P. Caradonna, Compton scattering mediated by quantum entanglement, Phys. Rev. A **111**, 053708 (2025).

[24] P. Caradonna and K. Shimazoe, Polarization symmetry as a signature of Bell states in Compton scattering, Phys. Rev. Res. **8**, 023288 (2026).

[25] M. H. L. Pryce and J. C. Ward, Angular correlation effects with annihilation radiation, Nature (London) **160**, 435 (1947).

[26] P. Caradonna, Kinematic analysis of multiple Compton scattering in quantum-entangled two-photon systems, Ann. Phys. **470**, 169779 (2024).